Published in final edited form as:
Cell Motil Cytoskeleton. 2008 September ; 65(9): 747–761. doi:10.1002/cm.20299.

Role of Nonmuscle Myosin IIB and N-RAP in Cell Spreading and Myofibril Assembly in Primary Mouse Cardiomyocytes

Shajia Lu and **Robert Horowits***
Laboratory of Muscle Biology, National Institute of Arthritis and Musculoskeletal and Skin Diseases, National Institutes of Health, Department of Health and Human Services, Bethesda, MD 20892

Abstract

We investigated the role of nonmuscle myosin heavy chain (NMHC) IIB in cultured embryonic mouse cardiomyocytes by specific knockdown using RNA interference. NMHC IIB protein levels decreased 90% compared with mock-transfected cells by 3 days post transfection. NMHC IIB knockdown resulted in a slow decrease in N-RAP protein levels over 6 days with no change in N-RAP transcript levels. N-RAP is a scaffold for α-actinin and actin assembly during myofibrillogenesis, and we quantitated myofibril accumulation by morphometric analysis of α-actinin organization. Between 3 and 6 days, NMHC IIB knockdown was accompanied by the abolishment of cardiomyocyte spreading. During this period the rate of myofibril accumulation steadily decreased, correlating with the slowly decreasing levels of N-RAP. Between 6 and 8 days NMHC IIB and N-RAP protein levels recovered, and cardiomyocyte spreading and myofibril accumulation resumed. Inhibition of proteasome function using MG132 led to accumulation of excess N-RAP, and the secondary decrease in N-RAP that otherwise accompanied NMHC IIB knockdown was abolished. The results show that NMHC IIB knockdown led to decreased N-RAP levels through proteasome-mediated degradation. Furthermore, these proteins have distinct functional roles, with NMHC IIB playing a role in cardiomyocyte spreading and N-RAP functioning in myofibril assembly.

Keywords

myofibrillogenesis; RNA interference; heart; sarcomere

Introduction

Nonmuscle myosin II has been implicated in a wide variety of cellular processes, including cell migration, establishment of cell polarity, cytokinesis, and cell-cell adhesion (reviewed in (Conti and Adelstein 2008)). In mice and humans, three genes encode the nonmuscle myosin II heavy chains, termed NMHC IIA, NMHC IIB, and NMHC IIC. Like muscle myosin, the nonmuscle myosins contain a catalytic head domain that functions as a molecular motor and a rod domain that forms a helical coiled coil dimer responsible for forming polymeric filaments (Sellers 2000; Straussman et al. 2005). Each NMHC also contains a short nonhelical tail region at its C-terminus (Hodge et al. 1992).

Although both NMHC IIA and IIB are expressed in skeletal muscle and heart tissues, only NMHC IIB appears to be present in cardiomyocytes, while NMHC IIA expression in the heart is restricted to blood vessels and capillaries (Murakami et al. 1993; Takeda et al. 2000). NMHC

*Address for Correspondence: Dr. Robert Horowits, Building 50, Room 1154, MSC 8024, National Institutes of Health, Bethesda, MD 20892-8024, Telephone: 301-435-8371, Fax: 301-402-0009, E-mail: horowits@helix.nih.gov.

IIC is also expressed in striated muscles (Golomb et al. 2004), but its distribution among cell types has not been reported. Isoform specific gene targeting of nonmuscle myosins in mice has demonstrated distinct critical roles for NMHC IIA and IIB during development. NMHC IIA knockout leads to early embryo death due to cellular and tissue disarray caused by widespread defects in cell-cell adhesion (Conti et al. 2004). In contrast, NMHC IIB knockout mice exhibit specific defects in cardiac development arising from cardiomyocyte hypertrophy accompanied by defective cytokinesis (Takeda et al. 2003; Tullio et al. 1997).

Interestingly, NMHC IIB has been localized at cardiac intercalated disks (Takeda et al. 2000) as well as in premyofibril structures, and has been hypothesized to be necessary for normal myofibril assembly (Du et al. 2003; Rhee et al. 1994). In cultured cardiomyocytes, prevention of nonmuscle myosin assembly into filaments by treatment with a kinase inhibitor was associated with the disappearance of myofibril precursors, further implicating NMHC IIB in myofibril assembly (Du et al. 2003). However, hearts of NMHC IIB knockout mice did assemble myofibrils, even though defects in cytokinesis and organ formation proved lethal within a day after birth (Takeda et al. 2003; Tullio et al. 1997).

The mechanism of myofibril assembly has been the subject of much research, leading to a number of models describing the specific sequence of events by which actin filaments, myosin filaments, and titin filaments assemble into linear arrays of sarcomeres (Gregorio and Antin 2000; Sanger et al. 2005). The earliest myofibril precursors appear near the cell periphery as immature fibrils containing punctate α-actinin Z-bodies, α-actin and muscle tropomyosin (Dabiri et al. 1997; Dlugosz et al. 1984; Ehler et al. 1999; Handel et al. 1991; Imanaka-Yoshida 1997; Lu et al. 2005; Rhee et al. 1994; Rudy et al. 2001; Schultheiss et al. 1990; Wang et al. 1988). Nonmuscle myosin IIB is also present between the Z-bodies of premyofibrils and and the Z-lines of nascent sarcomeres, but is gradually replaced by muscle myosin as the precursors assemble into the mature myofibril (Rhee et al. 1994).

In addition to nonmuscle myosin IIB, several other proteins are transiently associated with myofibril precursors during assembly (Greenberg et al. 2008). These include N-RAP, a molecular scaffold that promotes assembly of α-actinin and actin into I-Z-I structures in the first steps of myofibril assembly (Carroll et al. 2004; Carroll et al. 2001), and Krp1, which subsequently promotes lateral fusion of myofibril precursors (Greenberg et al. 2008). Interestingly, N-RAP knockdown by RNA interference halted myofibril assembly and lead to a decrease in NMHC IIB by post-transcriptional mechanisms (Dhume et al. 2006).

Here we probe the role of NMHC IIB and its relation to N-RAP levels by directly targeting this gene for knockdown in cultured cardiomyocytes using RNA interference. The present study demonstrates that NMHC IIB knockdown leads to decreased N-RAP levels through proteasome-mediated degradation. Furthermore, the slower rate of N-RAP degradation allowed us to assign separate functional roles for NMHC IIB and N-RAP in cardiomyocyte biology, with NMHC IIB playing a role in cardiomyocyte spreading and N-RAP functioning in myofibril assembly.

Materials and Methods

Primary Culture and Transfection of Embryonic Mouse Cardiomyocytes

Primary cultures of mouse cardiomyocytes were prepared from E17.5 CD-1 mouse embryos with minor modifications of previously described methods (Carroll and Horowits 2000; Dhume et al. 2006). Briefly, 50–90 hearts were minced and sequentially digested with 0.25% trypsin (Gibco) and 0.2% collagenase type II (Sigma). Cells were preplated onto tissue culture dishes (Falcon) to remove fibroblasts, which preferentially adhere to the plastic surface. The cardiomyocyte-enriched cultures were plated onto laminin-coated (Invitrogen) dishes or slides

at a density of 3.0–4.5 × 10^4 cells per cm^2. Growth medium consisted of 25 mM glucose DMEM lacking L-glutamine (Gibco) supplemented with 10% fetal bovine serum (Hyclone) and 1% gentamycin, 1% penicillin/streptomycin, and 1% antimycotic (all from Gibco).

Duplex siRNA targeted against NMHC IIB (5′-AAGGACCGCUACUAUUCAGGA-3′) and nonsense control siRNA duplex (5′-AAUUCUCCGAACGUGUCACGU-3′) were purchased from Qiagen (Valencia, CA). This NMHC IIB siRNA (with the underlined nucleotide substituted with U to account for variation between mouse and human sequence) has previously been found to specifically target this isoform of nonmuscle myosin in COS-7 cells (Bao et al. 2005). Cardiomyocytes were transfected with 20 nM siRNA 24 hrs after plating using HiPerFect transfection reagent (Qiagen, Inc) at 0.4% according to the manufacturer's protocol. Mock-transfected controls were treated identically except for the omission of siRNA. Transfection efficiency was ~90% as measured using Cy3-labeled nonsense control siRNA (Qiagen) as previously described (Dhume et al. 2006).

For some experiments cardiomyocytes were treated with the proteasome inhibitor MG132 (Alexis Biochemicals, San Diego, CA). Primary cultured mouse cardiomyocytes were transfected with siRNA 24 hrs after plating. MG132 was added to the culture medium at a final concentration of 0.3 μM or 1.0 μM at post-transfection day 3 and cells were grown for an additional 64 hrs.

RNA Isolation and Real-Time PCR

Total RNA was extracted and purified using the RNeasy Mini Kit (Qiagen, Valencia, CA) followed by on-column DNase digestion (Qiagen). First-strand cDNA was synthesized from 200 ng total RNA using the Advantage RT-for-PCR Kit (BD Biosciences, Palo Alto, CA) as per the manufacturer's protocol. Gene expression was quantitated using the MX3000p Real-time PCR System (Stratagene, Cedar Creek, TX) in combination with the Brilliant SYBR Green QPCR Master mix (Stratagene). PCR conditions and primers for NMHC IIB, N-RAP, α-actinin, Krp1, cardiac myosin heavy chain (MHC), MLP and 18s rRNA were as previously described (Dhume et al. 2006). NMHC IIC mRNA was amplified using previously described forward (5′-GCCCATGTGGCATCATCTCCA-3′) and reverse (5′-CTCCCACGATGTAGCCAGCA-3′) primers (Golomb et al. 2004) and the following amplification conditions: One cycle at 95°C for 10 minutes; 40 cycles at 95°C for 30 seconds, 56°C for 1 minute, then 72°C for 30 seconds.

The data were analyzed using the comparative C_T method (Giulietti et al. 2001; Livak and Schmittgen 2001). Gene expression was normalized to 18s rRNA expression in the same sample, and the normalized values from transfected cells were expressed as a fraction of the normalized values in mock-transfected controls prepared simultaneously.

Protein Isolation and Immunoblotting

Protein isolation, electrophoresis, and immunoblotting were performed as previously described (Dhume et al. 2006). Primary polyclonal antibodies against NMHC IIB (Covance, Emeryville, CA) and N-RAP (Luo et al. 1997) were diluted 1:2000. Primary monoclonal antibodies against sarcomeric actin (clone 5C5) and sarcomeric α-actinin (clone EA-53) were diluted 1:500 (Sigma-Aldrich, St. Louis, MO). Primary monoclonal antibodies against muscle MHC (clone MF20, Developmental Studies Hybridoma Bank of the University of Iowa) and GAPDH (clone 6C5, Abcam) were diluted 1:5000. Monoclonal anti-ubiquitin antibody was diluted 1:1000 (clone P4D1, Covance). Primary antibodies were detected with horseradish peroxidase-linked anti-rabbit and anti-mouse whole antibodies (Pierce, Rockford, IL). Protein levels were quantitated by densitometric analysis and normalized to GAPDH in the same samples.

Immunofluorescence Staining and Confocal Microscopy

Cultures were fixed and stained for immunofluorescence as previously described (Carroll and Horowits 2000; Dhume et al. 2006), with double staining accomplished by sequential incubation with primary antibodies. Polyclonal antibodies against NMHC IIB (Covance, Emeryville, CA) and N-RAP (Luo et al. 1997) were diluted 1:500 and 1:1000, respectively. Monoclonal antibodies against sarcomeric α-actinin (clone EA-53, Sigma-Aldrich, St. Louis, MO) were diluted 1:2000. Monoclonal antibodies against NMHC IIB (clone CMII23, used only for double labeling with polyclonal anti-N-RAP), fast muscle MHC (clone F59) and myomesin (clone B4) were obtained from the Developmental Studies Hybridoma Bank of the University of Iowa and used at 1:100, 1:100 and 1:200 dilutions, respectively. The polyclonal primary antibodies were detected using an Alexa fluor 488-linked goat anti-rabbit IgG secondary antibody (Invitrogen, CA) diluted 1:500. The monoclonal primary antibodies were detected using an Alexa fluor 568-linked goat anti-mouse IgG secondary antibody (Invitrogen, CA) diluted 1:1000 for α-actinin and 1:500 for muscle MHC and myomesin. Actin filaments were detected by staining for 30 minutes with AlexaFluor 488-labeled phalloidin (Invitrogen) diluted 1:100.

Images were collected using a Zeiss LSM 510 META laser scanning confocal microscope with 63X or 40X, 1.4 N.A. oil immersion objectives (Carl Zeiss, Thornwood, NY). Mean cell areas and myofibril areas were obtained by morphometric analysis performed using Image J software as previously described (Carroll et al. 2004; Carroll et al. 2001).

Nonmuscle Myosin IIB Tail Binding to Blotted Proteins

Recombinant histidine-tagged mouse N-RAP fragments N-RAP-LIM, N-RAP-IB and N-RAP-SR and histidine-tagged chloramphenicol acetyltransferase proteins HIS-CAT-1 and HIS-CAT-2 were prepared as previously described (Luo et al. 1999; Zhang et al. 2001). A histidine-tagged fragment containing 19 modules from the central super repeat region of mouse nebulin was generated by PCR directional subcloning of the nebulin 8c construct from the pTrxFus vector (Zhang et al. 1998) into the pProEX-1 vector. The forward primer was 5′-CATATGGGAATTCAACCTGCCGACATGCTGAGCGTCAC-3′, and the reverse primer was 5′-TCTAGAGGATCCCTAGCCGCATGTCATAGCCTTTCCTCT-3′. EcoR1 and BamH1 restriction sites used for cloning are underlined. All histidine-tagged proteins were expressed in *E. coli* and purified as previously described (Luo et al. 1999; Zhang et al. 2001).

A pET21c plasmid construct encoding the C-terminal 640 amino acids of human NMHC IIB was generously provided by Dr. Shoshana Ravid (The Hebrew University, Jerusalem, Israel). Recombinant NMHC IIB rod was expressed and purified from this construct essentially as described (Straussman et al. 2007).

Gel overlay binding assays were performed as previously described (Zhang et al. 2001). In brief, histidine-tagged recombinant proteins were electrophoresed under denaturing conditions and blotted to PVDF membranes. After washing and blocking, the membranes were incubated with 2.5 μg/ml (33 nM monomer or 17 nM if dimerized) NMHC IIB rod in binding buffer (100 mM KCl, 50 mM Tris-HCl (pH 7.4), 1 mM EGTA, 2 mM $MgCl_2$, 2 mM ATP, 0.3 mM DTT, and 0.2% Tween-20) for one hour. Bound NMHC IIB rod was detected using a primary polyclonal antibody raised against a C-terminal peptide (Covance Inc. CA) followed by horseradish peroxidase conjugated anti-rabbit antibody (Pierce); the primary and secondary antibodies were diluted 1:3000 and 1:8000, respectively, in PBS containing 0.2% tween-20. The ECL western blot system was used for detection of bound antibody (Amersham Biosciences, Piscataway, NJ).

Results

Specificity and Time-course of NMHC IIB Targeting by RNA Interference

In order to investigate the role of NMHC IIB in myofibril assembly, we treated primary cultures of embryonic mouse cardiomyocytes with siRNA that has previously been shown to specifically target this isoform of nonmuscle myosin (Bao et al. 2005). NMHC IIB transcript levels were specifically decreased by ~85% compared with mock-transfected cells within 1 day after transfection with NMHC IIB siRNA, but were not affected by nonsense control siRNA (figure 1A). The NMHC IIB transcript levels remained low for 5 days, and then recovered to control levels on days 6 and 8. Messages encoding other cardiomyocyte proteins were not reduced, including mRNAs encoding other isoforms of myosin, N-RAP, and N-RAP binding partners α-actinin and Krp1 (figure 1B–F). In many cases these mRNAs were increased relative to mock-transfected controls, but these increases were statistically significant only for α-actinin on day 3 and N-RAP on day 8; in these cases treatment with control and NMHC IIB siRNAs yielded equivalent changes.

Immunoblot analysis showed that NMHC IIB protein was decreased by 80% within 3 days of siRNA treatment (figure 2). N-RAP levels were secondarily affected, steadily decreasing by ~80% over 6 days. Both NMHC IIB and N-RAP protein levels returned to normal after 8 days. In contrast, only small changes were observed in levels of sarcomeric α-actinin, actin, and muscle MHC throughout the experiment when compared with mock-transfected controls. However, absolute levels of these muscle-specific proteins decreased with time (figure 2A), likely due to fibroblast proliferation in the primary cultures (Greenberg et al. 2008).

Microscopic Analysis of NMHC IIB Knockdown in Cardiomyocytes

We verified NMHC IIB localization and knockdown in cardiomyocytes by confocal microscopy of cultured cells double labeled with antibodies against sarcomeric α-actinin and NMHC IIB. In control cardiomyocytes, NMHC IIB was present at the cell periphery in regions containing assembling premyofibrils characterized by closely spaced dots of α-actinin (figure 3A–C, G–I). NMHC IIB staining is dramatically decreased in many cardiomyocytes 3 days or 5 days after knockdown (figure 3D–F, J–L). Mature striations containing α-actinin are maintained in the absence of NMHC IIB, but by day 5 peripheral premyofibril areas are often absent (figure 3J).

As previously reported, N-RAP is present in assembling premyofibrils at the cell periphery, as well as at the ends of mature myofibrils (figure 4A–C). Five days after transfection with siRNA against NMHC IIB, decreased N-RAP protein levels were observed in cardiomyocytes by confocal microscopy. In some cells low levels of N-RAP were detected, and small areas of closely spaced α-actinin dots remained (figure 4D–F, arrow). In other cells N-RAP staining was reduced to much lower levels, with residual N-RAP staining detected at myobril ends (figure 4G–I). In these cases significant peripheral areas of diffuse α-actinin staining were sometimes observed, with no detectable N-RAP (figure 4G–I, arrow).

In contrast to defects in premyofibril accumulation, mature striations appear to be unaffected by NMHC IIB knockdown and the secondary decrease in N-RAP levels. Sarcomeric α-actinin, myosin and actin filaments all exhibit normal banding patterns within mature myofibrils 5–6 days after NMHC IIB knockdown (figure 4D–L).

We analyzed cell spreading and mature myofibril accumulation by morphometric analysis of confocal images collected from cardiomyocytes stained with antibodies against sarcomeric α-actinin, as previously described (Carroll et al. 2004; Carroll et al. 2001). Under the conditions of these experiments, mean cell area and mean myofibril area in mock-transfected cardiomyocytes each increased linearly with time over 8 days (figure 5A,B). However, NMHC

IIB knockdown resulted in decreased cell areas and myofibril areas beginning 5 days after transfection with siRNA. The data show a clear pause in cell spreading and myofibril accumulation between days 3 and 6, followed by a resumption of these processes between 6 and 8 days after exposure to NMHC IIB siRNA. The pause in cell spreading appeared to precede the pause in myofibril accumulation: Between day 3 and day 5 after treatment with NMHC IIB siRNA, the mean myofibril area significantly increased ($p < 0.05$), while the mean cardiomyocyte area did not change during this period (figure 5B versus 5A, open symbols). When myofibril area is normalized to cell area, no statistically significant difference is observed between control and NMHC IIB knockdown cells (figure 5C). Nevertheless, between 3 and 6 days post transfection, myofibril area as a percentage of total cell area is marginally greater in siRNA treated cardiomyocytes than in mock-transfected controls, consistent with continued myofibril assembly after cell spreading was arrested by NMHC IIB knockdown.

Further analysis of the morphometric data in figure 5A and figure 5B yields the rate of cell spreading and myofibril assembly during NMHC IIB knockdown. These are depicted in figures 6A and 6B, respectively, as bar graphs, with changes in NMHC IIB and N-RAP protein levels overlayed as closed and open circles. Figure 6A shows that the rapid drop in NMHC IIB levels at day 3 is accompanied by a total cessation of cardiomyocyte spreading. The rate of myofibril accumulation slows more gradually, tracking the secondary decrease in N-RAP levels that accompany NMHC IIB knockdown (figure 6B). The rates of cardiomyocyte spreading and myofibril assembly both return to control levels between days 6 and 8, as both NMHC IIB and N-RAP increase to near normal levels.

N-RAP Degradation Through the Ubiquitin/Proteasome Pathway

Previous investigators have demonstrated that N-RAP binds MURF-1, a muscle RING finger protein that is a ubiquitin ligase controlling proteasome-dependent degradation of muscle proteins (Witt et al. 2005). Since N-RAP is decreased following NMHC IIB knockdown by a post-transcriptional mechanism, we explored the effects of proteasome inhibition on N-RAP levels. Treatment of cardiomyocytes with the proteasome inhibitor MG132 dramatically increased the total amount of ubiquitinated proteins detected by immunoblot using an anti-ubiquitin antibody (figure 7A). NMHC IIB levels decreased slightly in response to MG132, but knockdown by siRNA was not affected (figure 7B). In contrast, proteasome inhibition dramatically increased N-RAP levels, with 1 μM MG132 completely preventing any decrease in N-RAP levels in response to NMHC IIB knockdown (figure 7B). Levels of sarcomeric proteins exhibited smaller changes in response to proteasome inhibition, with α-actinin and muscle myosin increasing and actin remaining unchanged.

We localized the excess N-RAP that accumulates following proteasome inhibition by confocal microscopy. Following treatment with 0.3 μM MG132, N-RAP was localized in narrow bands bordering the Z-lines of mature myofibrils (figure 8A–F). Higher concentrations of MG132 lead to apparent disassembly of myofibrils, with N-RAP colocalizing with α-actinin in residual myofibrillar structures (figure 8G–L). These results were not affected by NMHC IIB knockdown (figure 8, D–F and J–L).

A possible mechanism for the mutual dependence of nonmuscle myosin IIB and N-RAP levels in cardiomyocytes is an interaction between the two proteins that protects both from degradation. Previous studies showed that the head region of muscle myosin binds nebulin repeats in vitro (Root and Wang 1994), but our previous work showed no direct binding between muscle myosin and N-RAP (Luo et al. 1999). Since nonmuscle myosin heavy chains contain unique C-terminal regions that are not present in muscle myosin (Hodge et al. 1992), we tested a recombinant C-terminal fragment of NMHC IIB for binding to N-RAP domains in a gel overlay assay. The NMHC IIB rod construct contains half of the coiled coil rod domain and the C-terminal 44 residues that comprise the nonhelical tailpiece (figure 9A). This NMHC

IIB construct bound to the N-RAP super repeats (N-RAP-SR) and N-RAP simple repeats (N-RAP-IB), as well as the N-RAP LIM domain (N-RAP-LIM) (figure 9B). Interestingly, the NMHC IIB rod construct also bound nebulin super repeats (neb 8c). Binding to the recombinant N-RAP and nebulin fragments was specific, as recombinant control proteins containing the same histidine tag present in the N-RAP and nebulin fragments (HIS-CAT-1 and HIS-CAT-2) did not bind NMHC IIB rod (figure 9B). In addition, incubating duplicate membranes without the NMHC IIB rod construct in the overlay buffer resulted in detection of only the NMHC IIB loaded onto the gel, with no detection of any of the recombinant N-RAP, nebulin or CAT proteins (data not shown).

In addition to interacting in vitro, NMHC IIB and N-RAP exhibit partial colocalization in cultured cardiomyocytes (figure 10). Although most of the NMHC IIB appears to be located more peripherally than most of the N-RAP, these proteins exhibit significant overlap in fibrillar structures located near the cell periphery (figure 10, insets 1 and 3) as well as the interior of the cell (inset 2).

Discussion

Role of Nonmuscle Myosin IIB in Cardiomyocyte Spreading

Gene targeting has demonstrated that nonmuscle myosin IIB is essential for normal cytokinesis and cardiac development in vivo (Takeda et al. 2003; Tullio et al. 1997). Using primary embryonic cardiomyocytes, we found that decreasing NMHC IIB levels by RNA interference is associated with a halt in cardiomyocyte spreading, a reduction in premyofibril content, and a decrease in the rate of myofibril accumulation. These effects are clearly linked to a primary reduction in NMHC IIB levels, as NMHC IIC mRNA measured by quantitative PCR (figure 1B) and NMHC IIA protein levels observed by immunoblot as well as staining in cardiomyocytes (data not shown) were unaffected. A secondary decrease in N-RAP levels was also observed. However, the halt in cell spreading clearly preceded the decrease in N-RAP levels, consistent with a primary mechanistic role for nonmuscle myosin IIB in cardiomyocyte spreading. This suggests that the cardiomyocyte hypertrophy observed in nonmuscle myosin IIB knockout mice is secondary to the defect in cytokinesis or to other factors that modulate organ formation in vivo (Takeda et al. 2003; Tullio et al. 1997).

Several recent studies have attempted to clarify the role played by nonmuscle myosin II isoforms in controlling cell size, shape, and migration. Knockdown studies in breast cancer and lung cancer cell lines implicate nonmuscle myosin IIB, but not IIA, in cell spreading (Betapudi et al. 2006; Sandquist et al. 2006). Migration was impaired by knockdown of either isoform in the breast cancer cells (Betapudi et al. 2006), but was impaired by NMHC IIB knockdown and enhanced by NMHC IIA knockdown in the lung carcinoma cells (Sandquist et al. 2006). In contrast, knockdown experiments revealed that NMHC IIA plays an important role in cell spreading in fibroblasts, while NMHC IIB does not (Cai et al. 2006). Finally, in CHO cells NMHC IIB knockdown was associated with an increase in cell area, and knockdown of either NMHC IIA or IIB increased rates of protrusion (Vicente-Manzanares et al. 2007). In the lung carcinoma cells, Rho kinase preferentially activated nonmuscle myosin IIA (Sandquist et al. 2006). In the fibroblasts, NMHC IIB was mainly concentrated in the center of the cell around the nucleus, while NMHC IIA was located along the dorsal surface and the peripheral ventral surface (Cai et al. 2006). It is clear from these studies that the role played by specific nonmuscle myosin II isoforms depends on differences in their subcellular localization and regulation, and that these factors may vary between cell types. Our finding that NMHC IIB plays a functional role in controlling cardiomyocyte size is consistent with its concentration at the cell periphery in spreading cardiomyocytes in culture (figure 3) (LoRusso et al. 1997; Rhee et al. 1994) as well as in developing precardiac organ culture (Du et al. 2003).

Post-Transcriptional Control of Nonmuscle Myosin and N-RAP Levels: Coordinated Regulation of Cell Size and Myofibril Assembly

NMHC IIB knockdown by siRNA resulted in a slow decrease in N-RAP protein levels by a post-transcriptional mechanism (figure 1D and figure 2B). Although there was a pause in both cardiomyocyte spreading and myofibril accumulation after NMHC IIB siRNA, these effects were temporally separated: While the halt in spreading was coincident with the initial decrease in NMHC IIB levels, the rate of myofibril accumulation steadily decreased as N-RAP levels fell (figure 5 and figure 6). The mean percentage of cardiomyocyte area filled with mature myofibrils was slightly elevated between 3 and 6 days following NMHC IIB siRNA (figure 5C), further supporting the interpretation that myofibrils continued to accumulate for a short period after cardiomyocyte spreading had stopped. The results show that although nonmuscle myosin IIB is essential for cardiomyocyte spreading, it is likely dispensable for myofibril assembly, consistent with findings from NMHC IIB knockout mice (Tullio et al. 1997). The decrease in myofibril accumulation that accompanies the secondary decrease in N-RAP levels is consistent with its proposed role as a scaffold for α-actinin and actin assembly into I-Z-I structures during myofibrillogenesis (Carroll et al. 2004; Carroll et al. 2001; Dhume et al. 2006).

The precise mechanism by which NMHC IIB knockdown leads to a decrease in N-RAP protein levels is unknown. However, proteasome inhibition dramatically increased N-RAP levels and prevented its decrease in response to NMHC IIB knockdown (figure 7). Although MG132 inhibits lysosomal as well as proteasome proteases (Lee and Goldberg 1998), N-RAP accumulation after proteasomal inhibition is consistent with N-RAP binding to the muscle ubiquitin ligase MURF-1 (Witt et al. 2005), a protein that has an anti-hypertrophic effect in the heart (Willis et al. 2007) and promotes atrophy in skeletal muscle (Bodine et al. 2001). NMHC IIB and N-RAP are partially colocalized in cardiomyocytes (figure 10), and the nonmuscle myosin IIB rod binds recombinant N-RAP fragments in vitro (figure 9), suggesting that direct interaction of these two proteins in the cardiomyocyte may protect N-RAP from degradation. A precedent for stabilization of a cytoskeletal protein by interaction with myosin has been demonstrated in *Dictyostelium*, where binding to myosin VII stabilizes cytosolic talin (Galdeen et al. 2007).

In summary, our findings show that NMHC IIB and N-RAP protein levels are tightly linked in cardiomyocytes, with decreases in either of these proteins leading to a decrease in the other by post-transcriptional mechanisms (figure 2B and (Dhume et al. 2006)). This has the functional consequence of linking cardiomyocyte spreading and myofibril assembly, allowing the cell to regulate the extent to which it is filled with myofibrils.

Acknowledgements

This research was supported by the Intramural Research Program of the National Institute of Arthritis and Musculoskeletal and Skin Diseases of the National Institutes of Health. We are grateful to Dr. Shoshana Ravid (The Hebrew University, Jerusalem) for the gift of expression plasmid encoding the NMHC IIB rod. We thank Drs. Evelyn Ralston and Kristien Zaal (Light Imaging Section, NIAMS) for instruction and guidance with the confocal microscopy. Finally, we thank Drs. Kuan Wang (NIAMS), Bob Adelstein (NHLBI), and Shoshana Ravid (The Hebrew University, Jerusalem) for helpful discussions and comments on the manuscript.

References

Bao J, Jana SS, Adelstein RS. Vertebrate nonmuscle myosin II isoforms rescue small interfering RNA-induced defects in COS-7 cell cytokinesis. J Biol Chem 2005;280(20):19594–19599. [PubMed: 15774463]

Betapudi V, Licate LS, Egelhoff TT. Distinct roles of nonmuscle myosin II isoforms in the regulation of MDA-MB-231 breast cancer cell spreading and migration. Cancer Res 2006;66(9):4725–4733. [PubMed: 16651425]

Bodine SC, Latres E, Baumhueter S, Lai VK, Nunez L, Clarke BA, Poueymirou WT, Panaro FJ, Na E, Dharmarajan K, et al. Identification of ubiquitin ligases required for skeletal muscle atrophy. Science 2001;294(5547):1704–1708. [PubMed: 11679633]

Cai Y, Biais N, Giannone G, Tanase M, Jiang G, Hofman JM, Wiggins CH, Silberzan P, Buguin A, Ladoux B, et al. Nonmuscle myosin IIA-dependent force inhibits cell spreading and drives F-actin flow. Biophys J 2006;91(10):3907–3920. [PubMed: 16920834]

Carroll S, Lu S, Herrera AH, Horowits R. N-RAP scaffolds I-Z-I assembly during myofibrillogenesis in cultured chick cardiomyocytes. J Cell Sci 2004;117(1):105–114. [PubMed: 14657273]

Carroll SL, Herrera AH, Horowits R. Targeting and functional role of N-RAP, a nebulin-related LIM protein, during myofibril assembly in cultured chick cardiomyocytes. J Cell Sci 2001;114(Pt 23):4229–4238. [PubMed: 11739655]

Carroll SL, Horowits R. Myofibrillogenesis and formation of cell contacts mediate the localization of N-RAP in cultured chick cardiomyocytes. Cell Motil Cytoskeleton 2000;47(1):63–76. [PubMed: 11002311]

Conti MA, Adelstein RS. Nonmuscle myosin II moves in new directions. J Cell Sci 2008;121(Pt 1):11–18. [PubMed: 18096687]

Conti MA, Even-Ram S, Liu C, Yamada KM, Adelstein RS. Defects in cell adhesion and the visceral endoderm following ablation of nonmuscle myosin heavy chain II-A in mice. J Biol Chem 2004;279(40):41263–41266. [PubMed: 15292239]

Dabiri GA, Turnacioglu KK, Sanger JM, Sanger JW. Myofibrillogenesis visualized in living embryonic cardiomyocytes. Proc Natl Acad Sci U S A 1997;94(17):9493–9498. [PubMed: 9256510]

Dhume A, Lu S, Horowits R. Targeted disruption of N-RAP gene function by RNA interference: A role for N-RAP in myofibril organization. Cell Motil Cytoskeleton 2006;63:493–511. [PubMed: 16767749]

Dlugosz AA, Antin PB, Nachmias VT, Holtzer H. The relationship between stress fiber-like structures and nascent myofibrils in cultured cardiac myocytes. J Cell Biol 1984;99(6):2268–2278. [PubMed: 6438115]

Du A, Sanger JM, Linask KK, Sanger JW. Myofibrillogenesis in the first cardiomyocytes formed from isolated quail precardiac mesoderm. Dev Biol 2003;257(2):382–394. [PubMed: 12729566]

Ehler E, Rothen BM, Hämmerle SP, Komiyama M, Perriard J-C. Myofibrillogenesis in the developing chicken heart: assembly of the z-disk, m-line and thick filaments. Journal of Cell Science 1999;112:1529–1539. [PubMed: 10212147]

Galdeen SA, Stephens S, Thomas DD, Titus MA. Talin influences the dynamics of the myosin VII-membrane interaction. Mol Biol Cell 2007;18(10):4074–4084. [PubMed: 17671169]

Giulietti A, Overbergh L, Valckx D, Decallonne B, Bouillon R, Mathieu C. An overview of real-time quantitative PCR: applications to quantify cytokine gene expression. Methods 2001;25(4):386–401. [PubMed: 11846608]

Golomb E, Ma X, Jana SS, Preston YA, Kawamoto S, Shoham NG, Goldin E, Conti MA, Sellers JR, Adelstein RS. Identification and characterization of nonmuscle myosin II-C, a new member of the myosin II family. J Biol Chem 2004;279(4):2800–2808. [PubMed: 14594953]

Greenberg CC, Connelly PS, Daniels MP, Horowits R. Krp1 (Sarcosin) promotes lateral fusion of myofibril assembly intermediates in cultured mouse cardiomyocytes. Exp Cell Res 2008;314(5):1177–1191. [PubMed: 18178185]

Gregorio CC, Antin PB. To the heart of myofibril assembly. Trends Cell Biol 2000;10(9):355–362. [PubMed: 10932092]

Handel SE, Greaser ML, Schultz E, Wang SM, Bulinski JC, Lin JJ, Lessard JL. Chicken cardiac myofibrillogenesis studied with antibodies specific for titin and the muscle and nonmuscle isoforms of actin and tropomyosin. Cell Tissue Res 1991;263(3):419–430. [PubMed: 1878931]

Hodge TP, Cross R, Kendrick-Jones J. Role of the COOH-terminal nonhelical tailpiece in the assembly of a vertebrate nonmuscle myosin rod. J Cell Biol 1992;118(5):1085–1095. [PubMed: 1512291]

Imanaka-Yoshida K. Myofibrillogenesis in precardiac mesoderm explant culture. Cell Struct Funct 1997;22(1):45–49. [PubMed: 9113389]

Lee DH, Goldberg AL. Proteasome inhibitors: valuable new tools for cell biologists. Trends Cell Biol 1998;8(10):397–403. [PubMed: 9789328]

Livak KJ, Schmittgen TD. Analysis of relative gene expression data using real-time quantitative PCR and the 2(-Delta Delta C(T)) Method. Methods 2001;25(4):402–408. [PubMed: 11846609]

LoRusso SM, Rhee D, Sanger JM, Sanger JW. Premyofibrils in spreading adult cardiomyocytes in tissue culture: evidence for reexpression of the embryonic program for myofibrillogenesis in adult cells. Cell Motil Cytoskeleton 1997;37(3):183–198. [PubMed: 9227849][published erratum appears in Cell Motil Cytoskeleton 1997;38(3):310].

Lu S, Borst DE, Horowits R. N-RAP expression during mouse heart development. Dev Dyn 2005;233 (1):201–212. [PubMed: 15765519]

Luo G, Herrera AH, Horowits R. Molecular interactions of N-RAP, a nebulin-related protein of striated muscle myotendon junctions and intercalated disks. Biochemistry 1999;38(19):6135–6143. [PubMed: 10320340]

Luo G, Zhang JQ, Nguyen TP, Herrera AH, Paterson B, Horowits R. Complete cDNA sequence and tissue localization of N-RAP, a novel nebulin-related protein of striated muscle. Cell Motil Cytoskeleton 1997;38(1):75–90. [PubMed: 9295142]

Murakami N, Trenkner E, Elzinga M. Changes in expression of nonmuscle myosin heavy chain isoforms during muscle and nonmuscle tissue development. Dev Biol 1993;157(1):19–27. [PubMed: 8482409]

Rhee D, Sanger JM, Sanger JW. The premyofibril: evidence for its role in myofibrillogenesis. Cell Motil Cytoskeleton 1994;28(1):1–24. [PubMed: 8044846]

Root DD, Wang K. Calmodulin-sensitive interaction of human nebulin fragments with actin and myosin. Biochemistry 1994;33(42):12581–12591. [PubMed: 7918483]

Rudy DE, Yatskievych TA, Antin PB, Gregorio CC. Assembly of thick, thin, and titin filaments in chick precardiac explants. Dev Dyn 2001;221(1):61–71. [PubMed: 11357194]

Sandquist JC, Swenson KI, Demali KA, Burridge K, Means AR. Rho kinase differentially regulates phosphorylation of nonmuscle myosin II isoforms A and B during cell rounding and migration. J Biol Chem 2006;281(47):35873–35883. [PubMed: 17020881]

Sanger JW, Kang S, Siebrands CC, Freeman N, Du A, Wang J, Stout AL, Sanger JM. How to build a myofibril. J Muscle Res Cell Motil 2005;26(6–8):343–354. [PubMed: 16465476]

Schultheiss T, Lin ZX, Lu MH, Murray J, Fischman DA, Weber K, Masaki T, Imamura M, Holtzer H. Differential distribution of subsets of myofibrillar proteins in cardiac nonstriated and striated myofibrils. J Cell Biol 1990;110(4):1159–1172. [PubMed: 2108970]

Sellers JR. Myosins: a diverse superfamily. Biochim Biophys Acta 2000;1496(1):3–22. [PubMed: 10722873]

Straussman R, Ben-Ya'acov A, Woolfson DN, Ravid S. Kinking the coiled coil--negatively charged residues at the coiled-coil interface. J Mol Biol 2007;366(4):1232–1242. [PubMed: 17207815]

Straussman R, Squire JM, Ben-Ya'acov V, Ravid S. Skip residues and charge interactions in myosin II coiled-coils: implications for molecular packing. J Mol Biol 2005;353(3):613–628. [PubMed: 16181641]

Takeda K, Kishi H, Ma X, Yu ZX, Adelstein RS. Ablation and mutation of nonmuscle myosin heavy chain II-B results in a defect in cardiac myocyte cytokinesis. Circ Res 2003;93(4):330–337. [PubMed: 12893741]

Takeda K, Yu ZX, Qian S, Chin TK, Adelstein RS, Ferrans VJ. Nonmuscle myosin II localizes to the Z-lines and intercalated discs of cardiac muscle and to the Z-lines of skeletal muscle. Cell Motil Cytoskeleton 2000;46(1):59–68. [PubMed: 10842333]

Tullio AN, Accili D, Ferrans VJ, Yu ZX, Takeda K, Grinberg A, Westphal H, Preston YA, Adelstein RS. Nonmuscle myosin II-B is required for normal development of the mouse heart. Proc Natl Acad Sci U S A 1997;94(23):12407–12412. [PubMed: 9356462]

Vicente-Manzanares M, Zareno J, Whitmore L, Choi CK, Horwitz AF. Regulation of protrusion, adhesion dynamics, and polarity by myosins IIA and IIB in migrating cells. J Cell Biol 2007;176(5):573–580. [PubMed: 17312025]

Wang SM, Greaser ML, Schultz E, Bulinski JC, Lin JJ, Lessard JL. Studies on cardiac myofibrillogenesis with antibodies to titin, actin, tropomyosin, and myosin. J Cell Biol 1998;107(3):1075–1083. [PubMed: 3047149]

Willis MS, Ike C, Li L, Wang DZ, Glass DJ, Patterson C. Muscle ring finger 1, but not muscle ring finger 2, regulates cardiac hypertrophy in vivo. Circ Res 2007;100(4):456–459. [PubMed: 17272810]

Witt SH, Granzier H, Witt CC, Labeit S. MURF-1 and MURF-2 target a specific subset of myofibrillar proteins redundantly: towards understanding MURF-dependent muscle ubiquitination. J Mol Biol 2005;350(4):713–722. [PubMed: 15967462]

Zhang JQ, Elzey B, Williams G, Lu S, Law DJ, Horowits R. Ultrastructural and biochemical localization of N-RAP at the interface between myofibrils and intercalated disks in the mouse heart. Biochemistry 2001;40(49):14898–14906. [PubMed: 11732910]

Zhang JQ, Weisberg A, Horowits R. Expression and purification of large nebulin fragments and their interaction with actin. Biophys J 1998;74(1):349–359. [PubMed: 9449335]

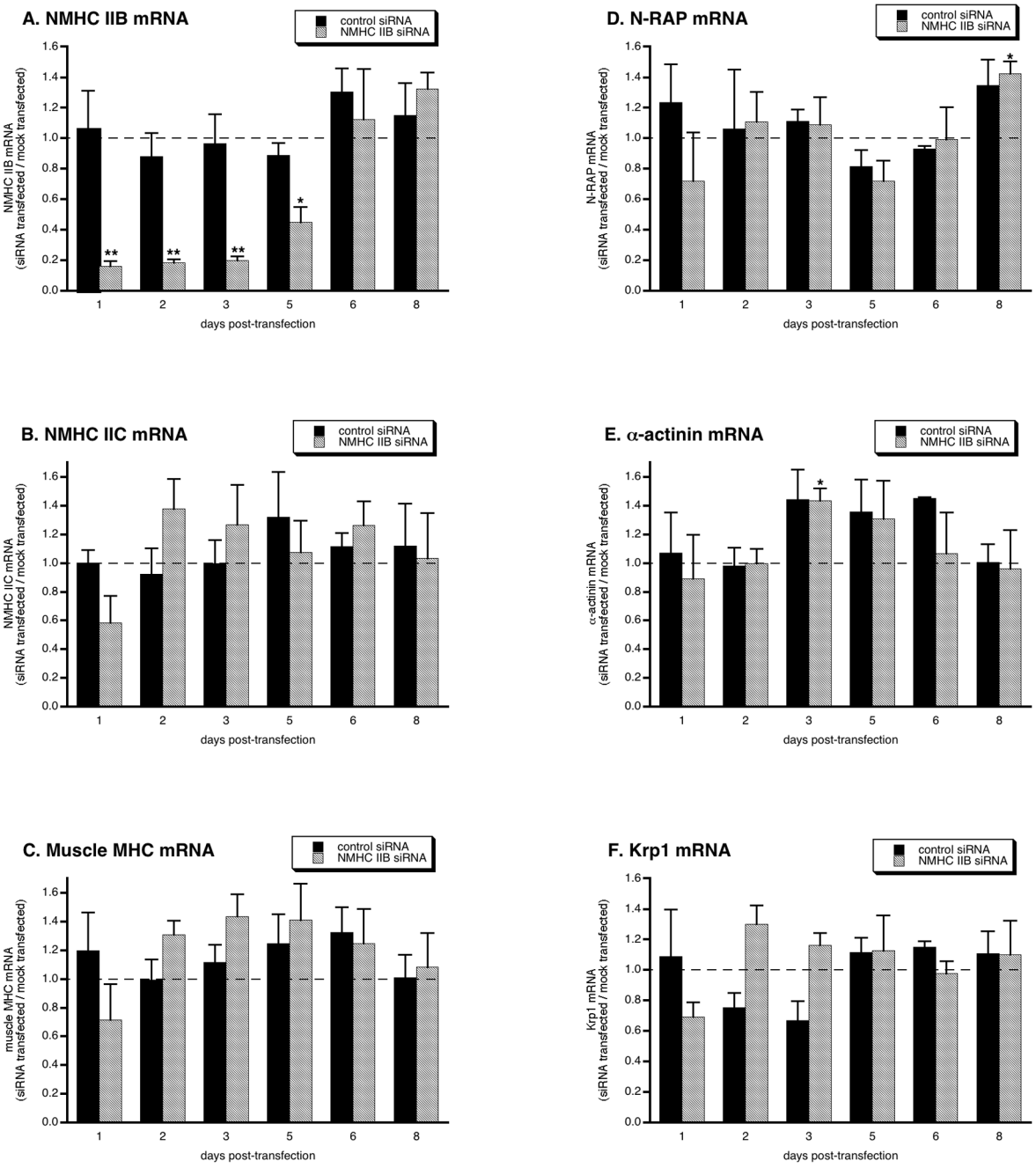

Figure 1.

Specific targeting of the NMHC IIB message by siRNA. mRNA levels were measured by real-time PCR at varying times after transfection with NMHC IIB siRNA or nonsense control siRNA. All values are expressed relative to levels measured simultaneously in mock-transfected controls (dashed lines). Each point is the mean and sem of three independent experiments. Asterisks indicate values significantly different from mock-transfected controls (*$p < 0.05$; **$p < 0.01$).

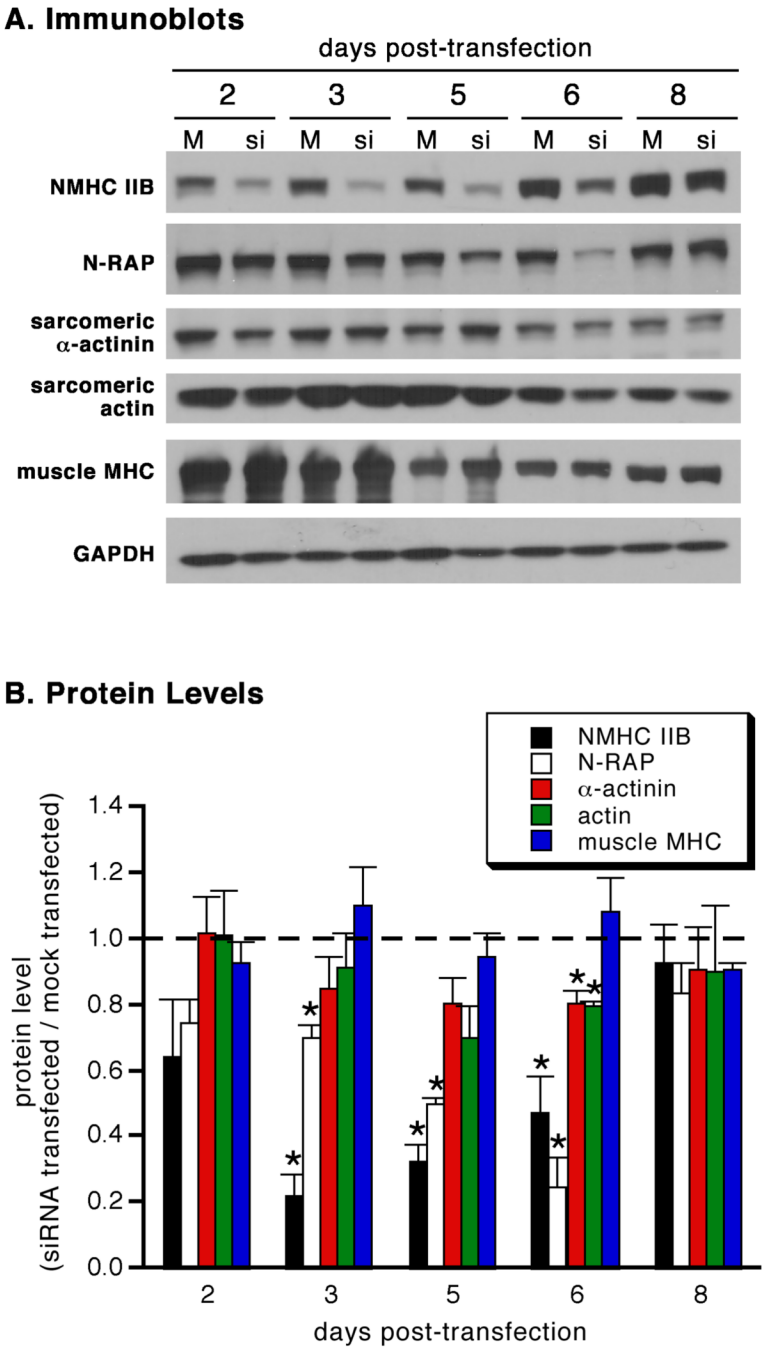

Figure 2.

Specificity of NMHC IIB protein knockdown by siRNA. (A) Immunoblots of mock-transfected (M) and NMHC IIB siRNA-transfected (si) cardiomyocytes. (B) Protein levels measured by densitometric analysis of immunoblots at varying times after transfection with NMHC IIB siRNA. All values are expressed relative to levels measured simultaneously in mock-transfected controls (dashed line). Each point is the mean and sem of three independent experiments. Asterisks indicate values significantly different from mock-transfected controls (*$p < 0.05$).

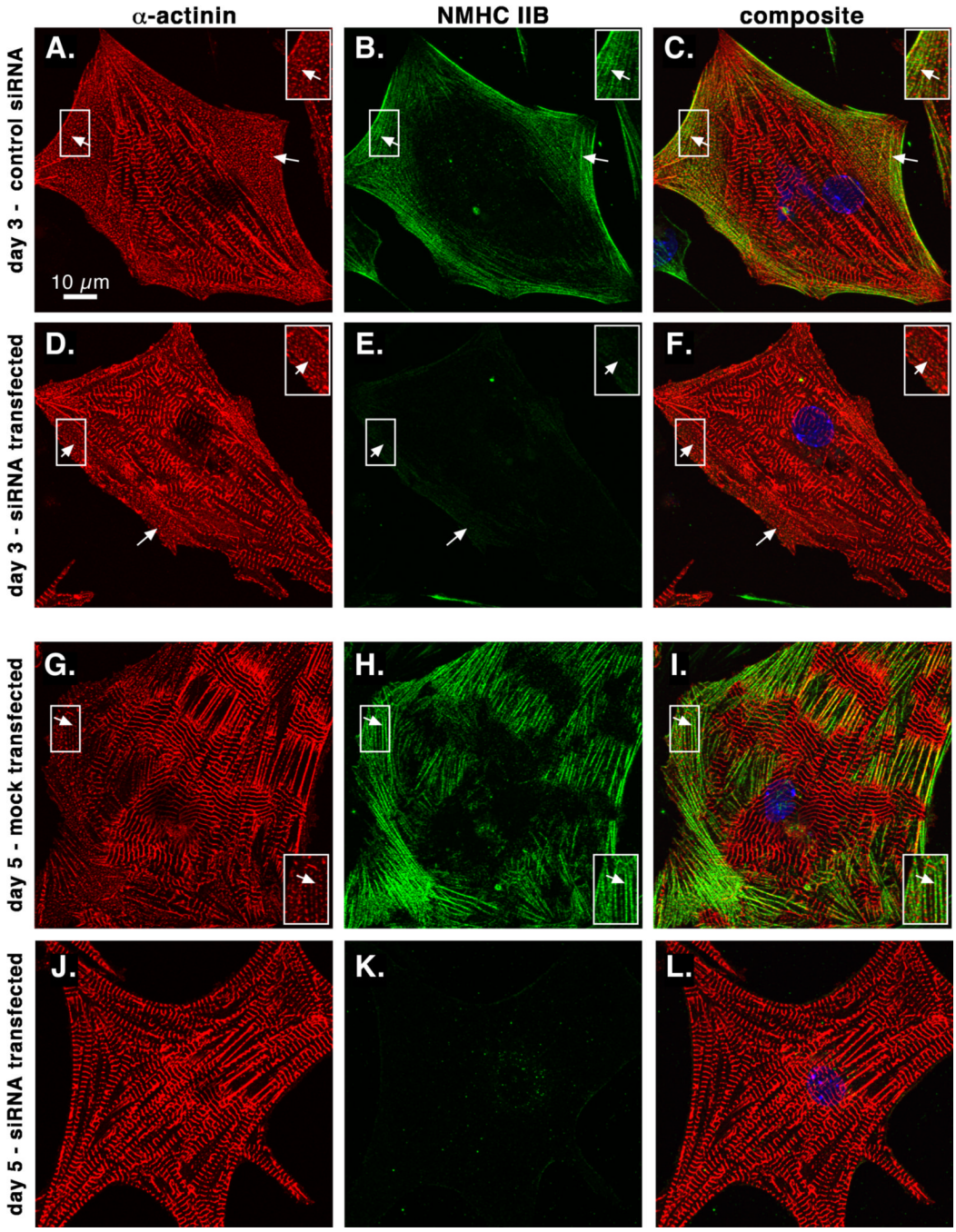

Figure 3.

NMHC IIB is reduced in cardiomyocytes by siRNA. Sarcomeric α-actinin (red) and NMHC IIB (green) were localized by double immunolabeling and confocal microscopy. Nonsense control siRNA-transfected (A–C), mock-transfected (G–I) and NMHC IIB siRNA-transfected (D–F and J–L) cardiomyocytes are shown 3 days (A–F) or 5 days (G–L) post-transfection. Note the concentrations of closely spaced α-actinin dots characteristic of assembling premyofibrils at the periphery of control cells (arrows, A–C and G–I) and after NMHC IIB knockdown at 3 days post-transfection (arrows, D–F), but their absence 5 days after siRNA treatment (J–L). Insets show boxed areas enlarged 50%.

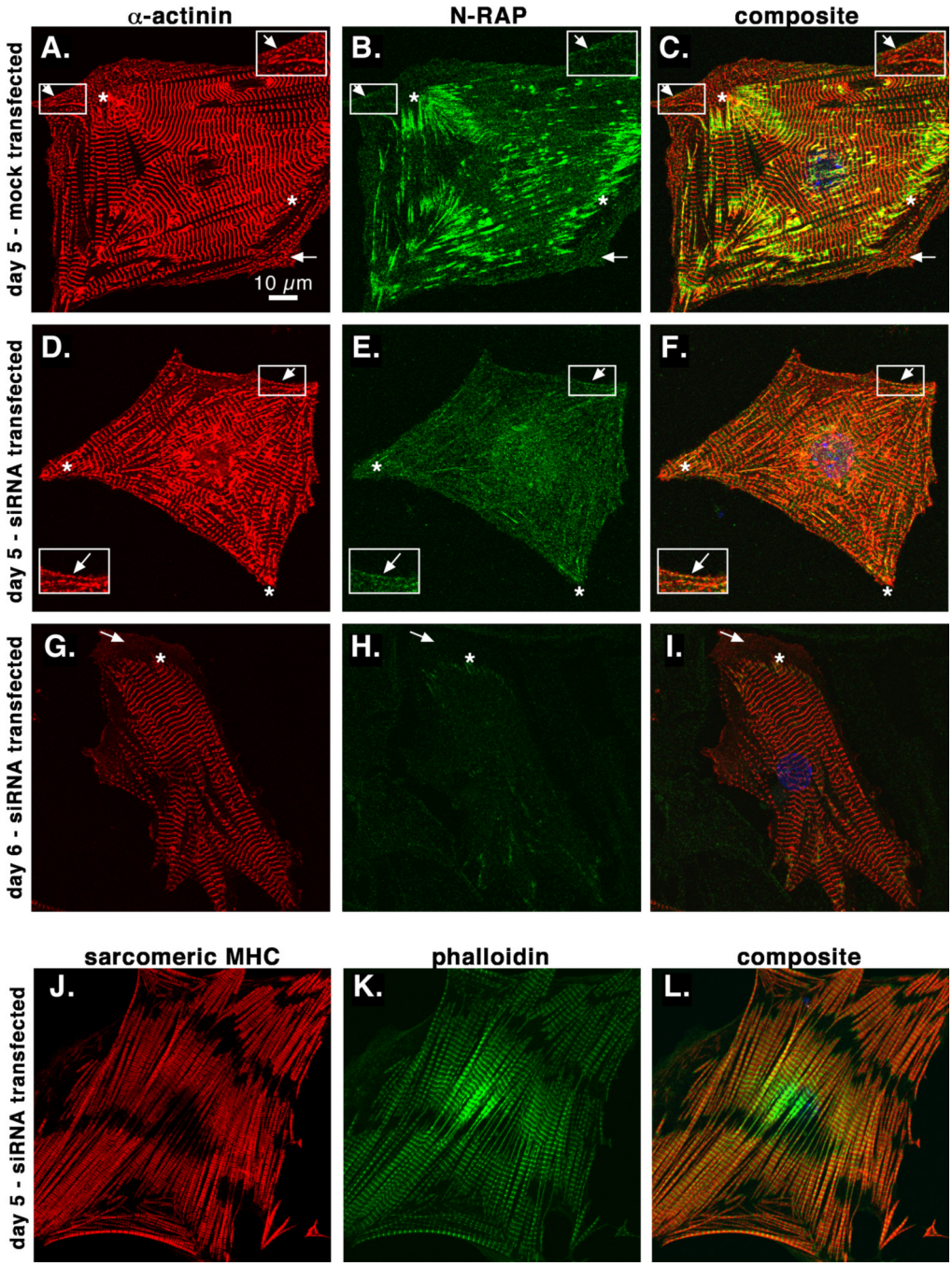

Figure 4.

N-RAP is reduced in cardiomyocytes after NMHC IIB knockdown. Sarcomeric α-actinin (red) and N-RAP (green) (A–I) or sarcomeric MHC (red) and actin filaments (green) (J–L) were localized by double labeling and confocal microscopy. Mock-transfected (A–C) and NMHC IIB siRNA-transfected (D–L) cardiomyocytes are shown 5 or 6 days after transfection, as indicated. Arrows indicate peripheral concentrations of closely spaced α-actinin dots characteristic of assembling premyofibrils in A–F, and a peripheral region of diffuse α-actinin staining in G–I. Asterisks mark accumulations of N-RAP at myofibril ends. Note the low level of N-RAP staining and the decreased occurence of peripheral α-actinin dots 5–6 days after

NMHC IIB knockdown (D–I), with normal sarcomeric organization of actin and myosin (J–L). Insets show boxed areas enlarged 50%.

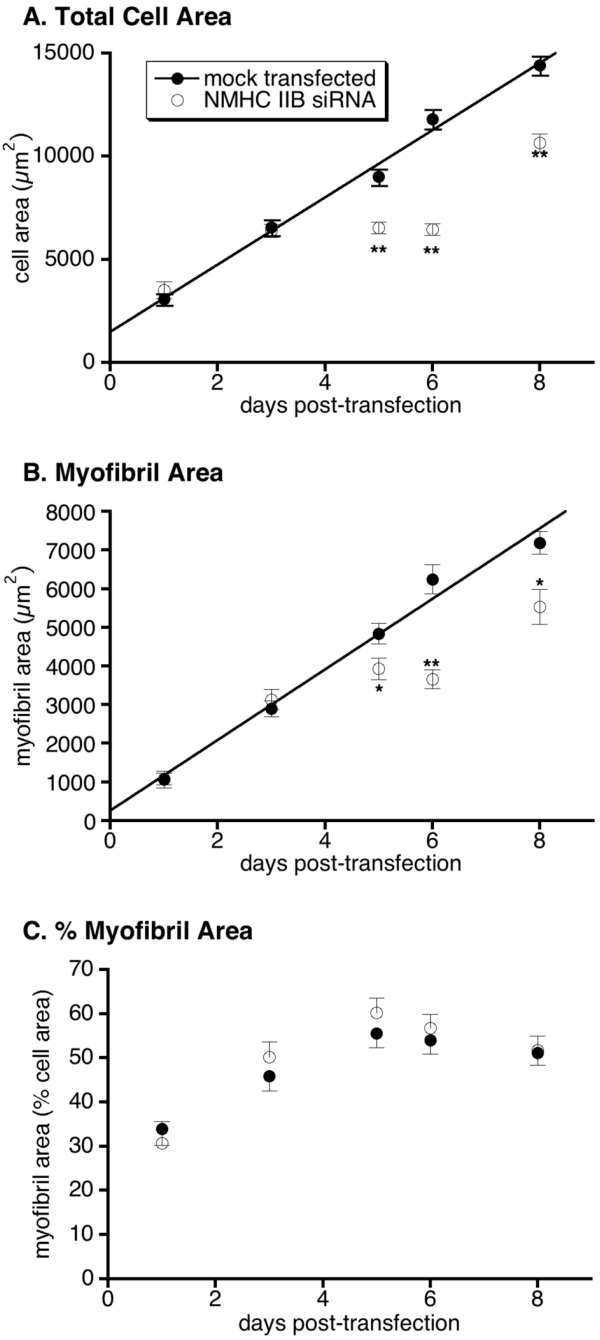

Figure 5.

Morphometric analysis of cardiomyocytes stained for sarcomeric α-actinin. Mean cell areas (A), mean myofibril areas (B), and mean myofibril areas expressed as a percentage of cell area (C) are shown at varying times after transfection. Each point is the mean and sem of 19–32 cardiomyocytes from 1–3 independent experiments. Asterisks indicate values significantly different from mock-transfected controls (*$p < 0.05$; **$p < 0.001$). Solid lines in A and B are linear fits to the mock-transfected data ($R > 0.99$ for both).

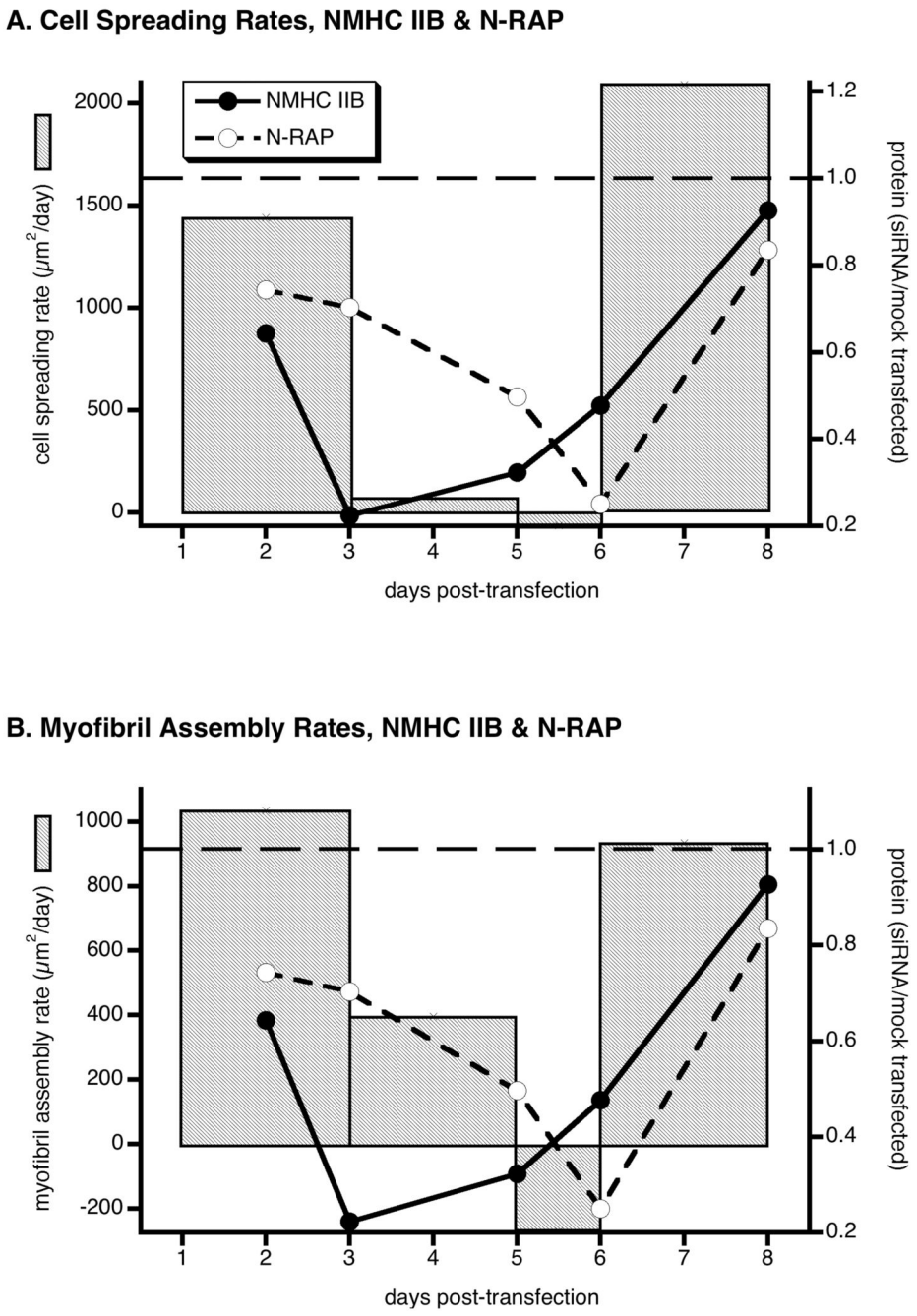

Figure 6.

Rates of cell spreading (A) and myofibril assembly (B) compared to changing NMHC IIB and N-RAP levels in response to NMHC IIB siRNA. The slopes of the mean cell area (A) and myofibril area (B) versus time data are plotted as bar graphs for cardiomyocytes after NMHC IIB knockdown. Horizontal dashed lines show the constant mean rates of cell spreading and myofibril assembly in mock-transfected cells for comparison. The mean levels of NMHC IIB (filled circles) and N-RAP (open circles) expressed relative to mock-transfected controls are also shown during the knockdown experiment. Morphometric and protein data axes are scaled so that the values in mock-transfected cells (horizontal dashed lines) coincide and the minimum measured values fall at the bottom of the scale. Rates of cell spreading and myofibril assembly

correspond to the slopes between time points in figures 5A and 5B, respectively. Protein levels are taken from figure 2B.

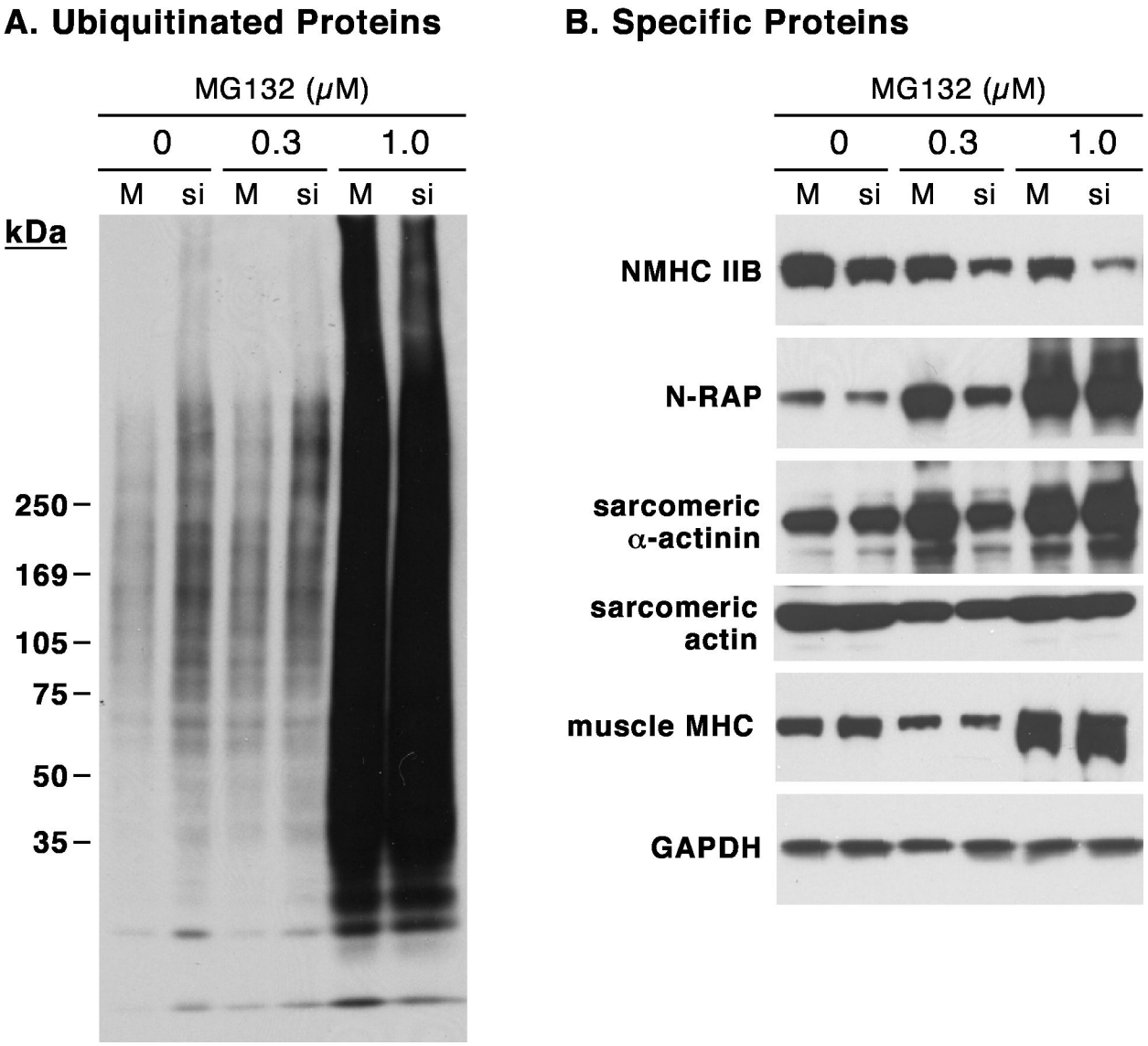

Figure 7.

Accumulation of ubiquitinated proteins and N-RAP after proteasome inhibition during NMHC IIB knockdown. Immunoblot detection of total ubiquitinated proteins (A) and NMHC IIB, N-RAP and major sarcomeric proteins (B) is shown after ~3 days of exposure to the indicated concentrations of MG132. Results are shown for mock-transfected (M) and NMHC IIB siRNA-transfected (si) cardiomyocytes 6 days after transfection.

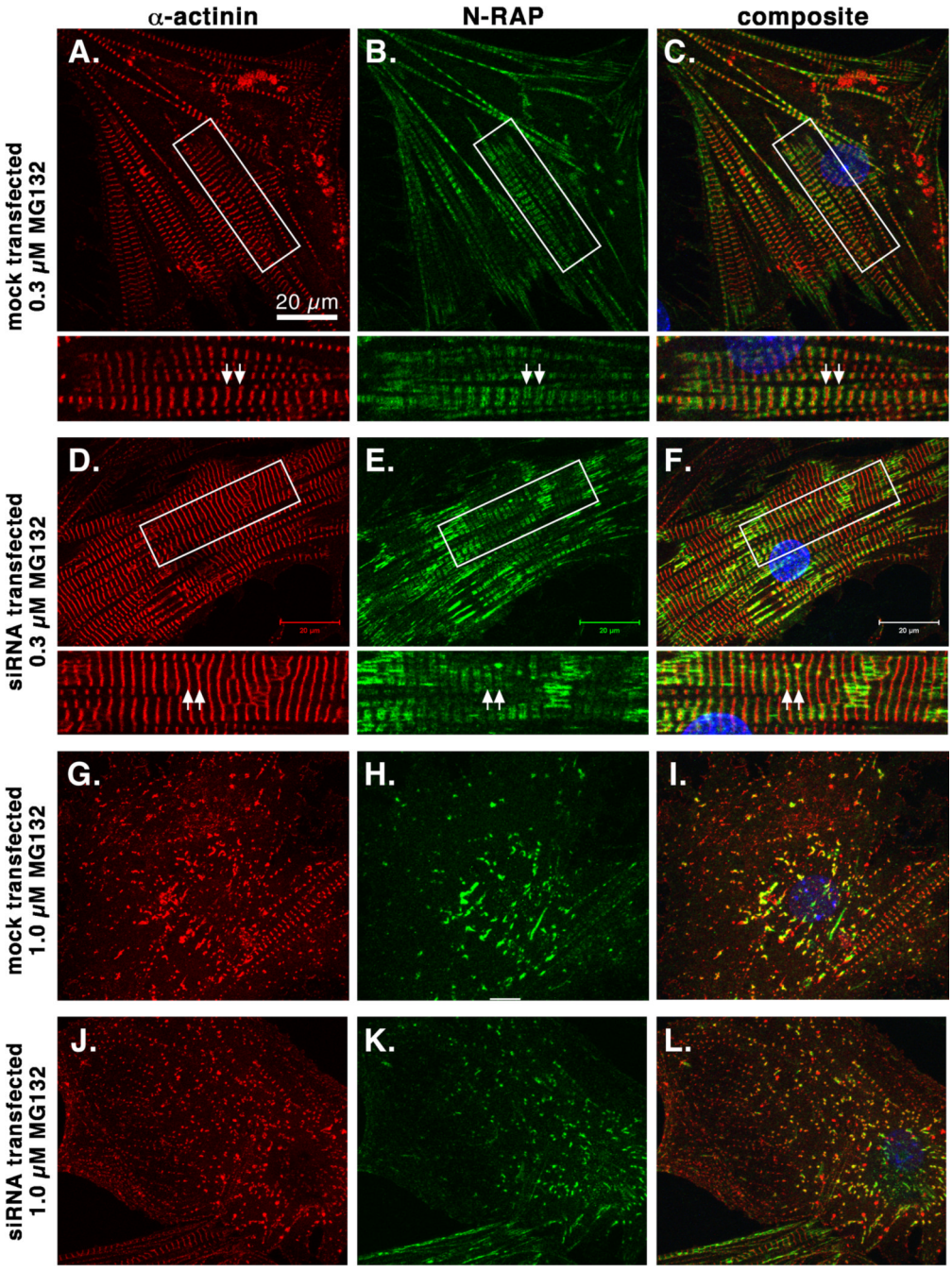

Figure 8.

Confocal imaging of cultured mouse cardiomyocytes double stained for sarcomeric α-actinin (red, left panels) and N-RAP (green, center panels) after proteasome inhibition by MG132. Examples of mock-transfected (A–C and G–I) and NMHC IIB siRNA treated (D–F and J–L) cardiomyocytes are shown after exposure to 0.3 μM (A–F) or 1.0 μM (G–L) MG132. Boxed areas in A–F are shown at higher magnification below the main panels. Note that after 0.3 μM MG132, N-RAP is observed in narrow bands bordering the Z-lines (A–F, arrows), but that after 1.0 μM MG132 N-RAP colocalizes with α-actinin in residual myofibrillar structures (G–L).

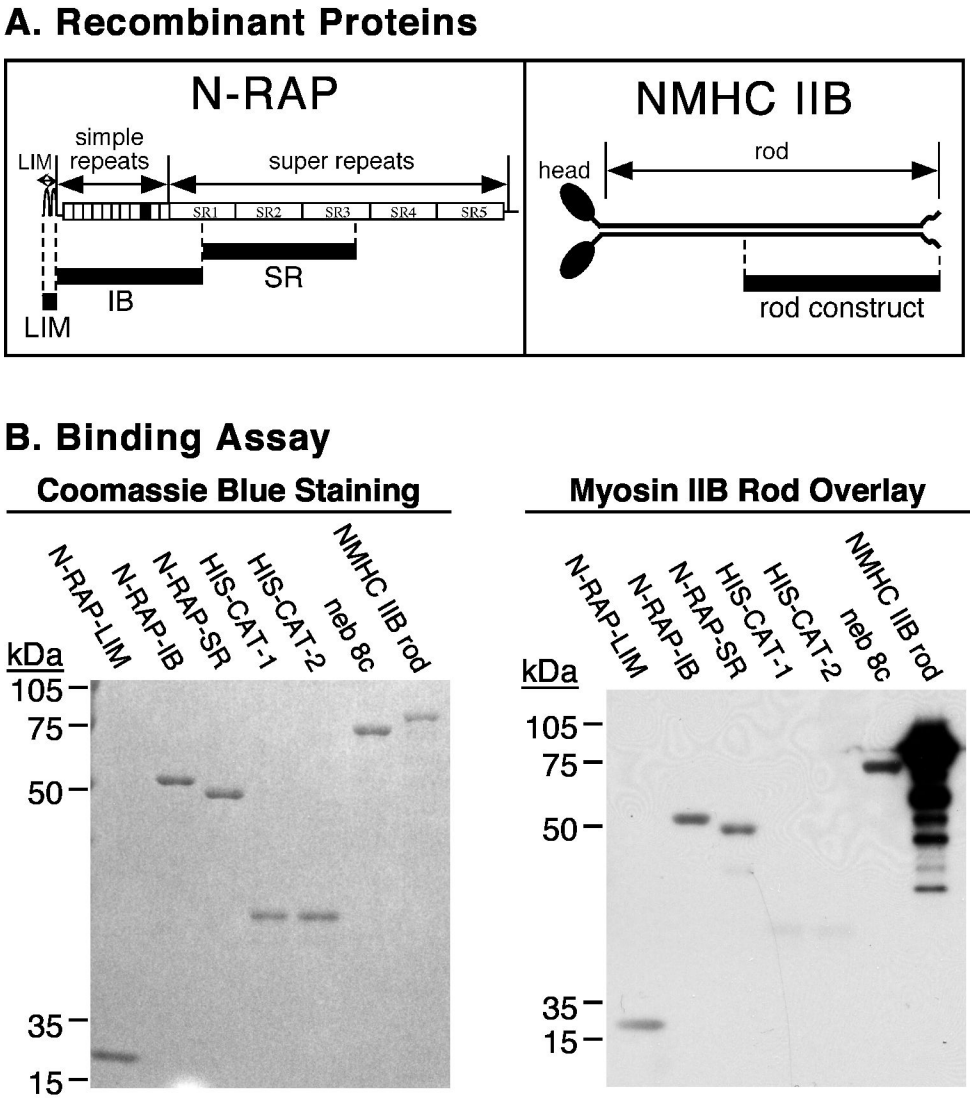

Figure 9.

NMHC IIB rod fragment binds N-RAP and nebulin fragments. (A) Diagram showing regions of N-RAP and NMHC IIB used for binding assays. (B) Purified recombinant proteins electrophoresed and detected with coomassie blue (left panel) or antibody detection of recombinant NMHC IIB rod bound to the indicated blotted proteins (right panel). Recombinant histidine-tagged CAT proteins (HIS-CAT-1 and HIS-CAT-2) served as negative controls. Significant nonmuscle myosin IIB tail binding was observed to each of the N-RAP fragments (N-RAP-LIM, N-RAP-IB, and N-RAP-SR) as well as to the nebulin super repeat construct (neb 8c). Incubating duplicate membranes without the NMHC IIB rod construct in the overlay buffer resulted in detection of only the NMHC IIB loaded onto the gel, with no detection of any of the recombinant N-RAP, nebulin or CAT proteins (data not shown).

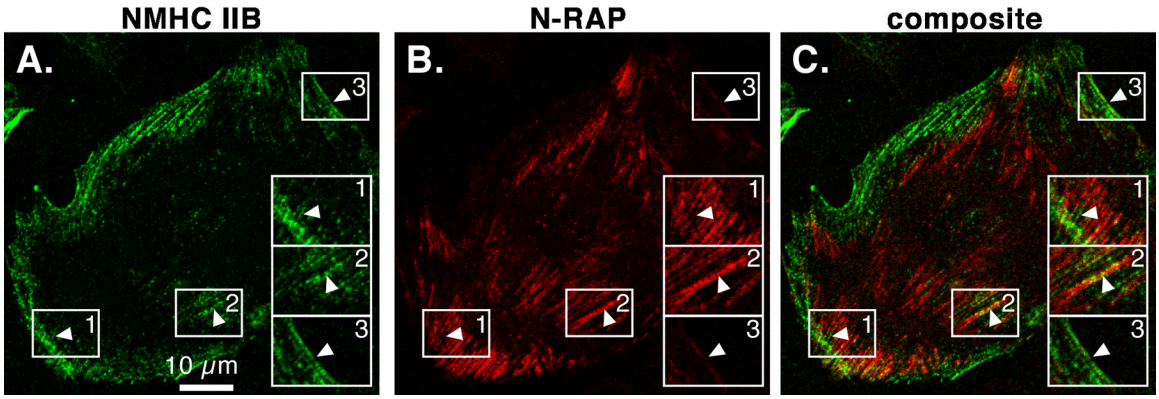

Figure 10.
Partial colocalization of NMHC IIB and N-RAP in cardiomyocytes. NMHC IIB (A, green) and N-RAP (B, red) were localized by double immunolabeling and confocal microscopy. Arrowheads indicate regions exhibiting colocalization. Insets show boxed areas enlarged 50%.